Available online at www.sciencedirect.com
ScienceDirect
Journal of Nuclear Materials 366 (2007) 353–368
journal of nuclear materials
www.elsevier.com/locate/jnucmat

Microstructural and mechanical property changes in the Ta-base T-111 alloy following thermal aging

Keith J. Leonard *, Jeremy T. Busby, Steven J. Zinkle

Materials Science and Technology Division, Oak Ridge National Laboratory, Oak Ridge, TN 37831, United States

Abstract

The microstructural changes occurring in the Ta-base T-111 (Ta–8W–2Hf) alloy during 1100 h thermal aging at 1098, 1248 and 1398 K under inert atmosphere and the influence on mechanical properties are reported. Electrical resistivity, hardness and tensile properties are compared between the as-annealed and aged conditions. Microstructural evaluations were performed by optical, scanning electron microscopy and transmission electron microscopy. An increase in the amount of grain boundary precipitation with increasing aging temperature was found to decrease the electrical resistivity and material strength. Precipitation at the grain boundaries was found to be a mixture of monoclinic and cubic structures, suggesting the development of mixed Hf oxides, carbides and nitrides. Precipitate development caused pronounced embrittlement of the alloy following aging at 1398 K.
Published by Elsevier B.V.

PACS: 81.40.Cd; 81.05.Bx; 89.30.Gg; 62.20.Fe

1. Introduction

Interest in fission reactor design concepts in support of higher performance, longer duration space exploration missions has led to frequent evaluations of refractory metal alloys to achieve the elevated temperature requirements of such missions. Of the possible Group V (V, Nb, Ta) and VI (Cr, Mo, W) refractory alloys, Ta-base T-111 (Ta + 8 wt% W + 2Hf) offers excellent formability and ductility at low temperatures, while showing good high temperature strength and alkali metal compatibility. Though tensile properties [1–10], creep testing [11–14], corrosion testing [15–17], and weldability studies [18–20] of T-111 have been investigated for different levels of cold work and annealing, bringing the technology to varying levels of maturity, the effects of aging on the mechanical properties is not as well understood. Earlier work on aging of T-111 under vacuum and liquid metal environments has shown conflicting results related to degradation in material ductility following exposure. It was observed by Watson and Stephens [21] and further by Stephens [22,23] that embrittlement occurred in material aged in a very narrow temperature range around 1310 K due to the formation of Hf-rich compounds at the grain boundaries. However, similar work by Lessmann and Gold [24] did not reveal any significant changes in material ductility.

* Corresponding author. Fax: +1 865 241 3650.
E-mail address: leonardk@ornl.gov (K.J. Leonard).

0022-3115/$ - see front matter Published by Elsevier B.V.
doi:10.1016/j.jnucmat.2007.03.026

The production of high-quality tantalum products has been well summarized [25]. The T-111 alloy was commercially available from several vendors in the 1960s [5]. However, developmental work on most refractory alloys including T-111 was halted in the early 1970s due to the suspension of funding for nuclear space power systems [26]. The T-111 samples of this present study, part of the recent NASA Prometheus Program, were fabricated from a 1960s heat of material as there is no current commercial vendor. It was the goal of this work to evaluate the changes in mechanical properties of T-111 as a result of aging at relevant space reactor temperatures between 1100 and 1400 K and to further provide experimental knowledge to the database of this alloy for evaluation of its use in high temperature applications. Characterization through the use of electron microscopy techniques of the microstructural changes influencing the mechanical properties were, for the first time, investigated.

2. Experimental

2.1. Sample fabrication

The T-111 alloy examined in this study was provided by Pittsburgh Materials Technology Inc. (PMTI), heat number 570–571, from a production run in the late 1960s. The measured composition of the alloy in the as-received condition and following thermal anneal and aging is presented in Table 1. Chemical analysis of the annealed and aged materials was provided by Wah Chang, while analysis of the as-received material was provided with the alloy by PMTI.

Miniature sheet tensile specimens of SS-3 geometry ($0.76 \times 1.52 \times 7.62$ mm gauge and 25.4 mm overall length) were fabricated from the as-received material using Mo-wire electrical discharge machining (EDM) with water as the cooling fluid to minimize impurity pickup. Specimens were cut so that the gage length of the tensile samples was parallel to the rolling direction of the sheet material. Following cutting, samples were polished to a 32 finish or better. After sample fabrication and prior to annealing, all samples were electrochemically cleaned for one minute in a solution of water, nitric acid, and hydrochloric acid [27].

2.2. Heat treatments

A total of 21 tensile and four metallographic T-111 samples were annealed for 1 h at 1883 K in high vacuum 1.3×10^{-4} Pa (1×10^{-6} Torr) prior to any long term aging. Specimens were placed inside a Nb–1Zr box in the furnace to reduce the potential for impurity pickup. Samples were furnace cooled under vacuum, by cutting current to the furnace elements; resulting in an approximate 160 K/min cooling rate from 1883 to 1473 K, 50 K/min from 1473 to 1073 K and less than 20 K/min below 1073 K.

The thermal aging treatments were conducted in support of irradiation experiments conducted at ORNL [28]. Therefore, the SS-3 samples were loaded into pure Nb holders held in place with Mo springs similar to their irradiated counterparts. The Nb holders, each containing three tensile specimens along with Ta foil wrapped metallurgical samples, were loaded into alumina tubes with alumina end-caps that were in turn placed in an alloy 600 tube and sealed with end caps. The superalloy capsules were welded shut under the same inert gas used in the irradiation study; helium for 1098 and 1248 K aging and neon for the 1398 K aging (based on heat transfer issues of the irradiated counterpart samples). Prior to welding, repeated pumping and purging cycles were performed to ensure a purified atmosphere in the encapsulated cans. During each pump cycle a vacuum of approximately 1.3×10^{-4} Pa (1×10^{-6} Torr) was obtained. Leak

Table 1
Measured compositions (in wt% or wppm) of T-111 in the as-received, annealed and aged conditions

Condition	Ta (wt%)	W (wt%)	Hf (wt%)	Zr (wt%)	C (wppm)	N (wppm)	O (wppm)	H (wppm)
As-received[a]	Bal.	8.40	2.05	–	45	27	65	–
Annealed 1 h at 1883 K[b]	Bal.	8.69	2.01	0.04	108	25	110	<3
Annealed + Aged 1100 h at 1098 K	Bal.	8.62	1.96	0.04	86	<20	70	<3
Annealed + Aged 1100 h at 1248 K	Bal.	8.72	1.99	0.04	81	<20	120	<3
Annealed + Aged 1100 h at 1398 K	Bal.	8.75	1.83	0.03	78	110	150	<3

[a] Chemical analysis provided by PMTI, 1960/1970 vintage analysis on original ingot.
[b] Al, B, Be, Co, Cr, Cu, Fe, Ni, Si, and Ti levels below 50 wppm.

checking of the sealed capsules was performed prior to aging for 1100 h in open air box furnaces at 1098, 1248 and 1398 K. The aging temperatures selected were 25 K higher than the designed irradiation temperatures used in the companion tests, based on the margin of uncertainty in the design irradiation temperatures. Temperatures in the box furnace were monitored by placing thermocouples located near the sealed capsules. The duration of all aging treatments was 1100 h.

Visual inspection of the samples aged at 1098 and 1248 K showed no signs of oxidation/nitridation. However, upon inspection of the 1398 K aging capsule, discoloration (oxidation/nitridation) was observed on the Ta foil and Nb holders. The discoloration appeared to be the result of a pinhole leak in the welded end cap of the alloy 600 can, estimated to have opened during cooling due to contractions of the capsule body. Further discoloration was observed on the edges of the SS-3 samples at the ends of the grip sections that were nearest to the open end of the Nb holder.

Chemical analysis of the impurity levels in the annealed and aged samples was performed at Wah Chang using inert gas fusion techniques for oxygen and nitrogen, and by combustion analysis for carbon. Chemical analysis of the as-received material was performed by PMTI and was provided with the alloy. The interstitial impurity elements in the material in the as-received condition and following the 1 h anneal and 1100 h aging treatments are presented in Table 1. Analysis of substitutional impurities (Al, B, Be, Co, Cr, Cu, Fe, Ni, Si, and Ti) in the annealed and aged alloy was also performed, with values remaining below the detectable 50 wppm level. Chemical analysis of the T-111 specimens showed an increase in nitrogen content after aging at 1398 K. While oxygen content was elevated, it was relatively unchanged from the annealed condition. The influence of this increase on the mechanical properties will be discussed later.

2.3. Microscopy and metallographic analysis

Pieces from the annealed and aged metallographic samples were polished and examined in a Philips XL30-FEG scanning electron microscope (SEM). The metallographic samples were then etched with a solution of 40 vol.% HCL + 20% mL HNO_3 + 40% HF and examined by optical microscopy (OM). Samples for transmission electron microscopy were cut by EDM and polished to less than 0.25 mm thickness and jet-polished with an electrolyte of 10 vol.% H_2SO_4 + 4% HF + 14% Butoxy Ethanol in methanol at 268 K. Samples were examined in a Philips Tecnai T20 and CM200 FEG transmission electron microscope (TEM) each equipped with energy dispersive X-ray spectrometer (EDS).

Hardness measurements were made on the annealed and aged tensile specimens using a Buehler Micromet 3 hardness indenter equipped with a Vickers indenter tip using a 1 kg load, with a dwell time of 15 s. One specimen was analyzed for each thermal treatment condition. At least seven measurements were made per sample on the grip regions of the SS-3 tensile specimens, well away from the gage length so that later tensile tests were not influenced.

2.4. Electrical resistivity

Electrical resistivity was measured at ambient temperature using a four-point probe technique on the standard SS-3 tensile specimens of each alloy in the as-annealed and aged conditions, in accordance with ASTM B 193-87 [29]. The measured voltage drop was readily converted to resistivity at a reference temperature of 294.6 K. The resistivity was calculated from the measured voltage drop using

$$\rho_{294.6}(\mathrm{n\Omega\,m}) = \frac{(V \times A)}{(I \times L)(1 + \alpha(T_{\mathrm{m}} - 294.6))}, \qquad (1)$$

where

- $\rho_{294.6}$ resistivity in nanoOhm m at the reference temperature of 294.6 K
- V measured voltage at the measurement temperature (in nanoVolts)
- A cross-sectional area of sample in m^2
- I applied current (0.1 A)
- L distance between inner electrodes = 0.00646 m for SS-3 sample holder
- α temperature coefficient of electrical resistivity
- T_{m} temperature of measurement (K).

For each specimen, the cross-sectional area was measured using a calibrated micrometer with 1 μm or better resolution. The width of the gage section was measured at the center of the gage section and the specimen thickness is measured at two locations along the gage length. The temperature was measured before and after electrical measurements on

each set of specimens. The temperature coefficient of electrical resistivity, α, was selected as 0.0035 K^{-1} which is the value for pure Ta [30].

2.5. Tensile properties

Tensile testing was performed on the as-annealed and aged SS-3 specimens following ASTM standard E8-04 [31]. Yield stress, ultimate tensile stress, and uniform and total elongation were determined for each test. Tests at room temperature and elevated temperatures were performed using a United Technology System SFM-10 test frame, equipped with a Thermal Technology vacuum furnace. Tensile tests were performed at a crosshead speed of 0.0076 mm/s (0.018 in/min), corresponding to a nominal strain rate of $\sim$0.001 s^{-1}. Testing of the aged samples was performed at the same targeted temperatures as their companion irradiated samples (1073, 1223, or 1373 K). Temperatures were measured using a type-C thermocouple positioned within 2 mm of the gauge section. Room temperature tests were conducted in air, while elevated temperature testing was in vacuum, maintained at 2.6×10^{-4} Pa (2×10^{-6} Torr) or lower.

3. Results and discussion

3.1. Microscopy

Optical (OM), SEM and TEM examination was performed on the as-annealed and aged samples. The as-annealed material consisted of an equiaxed grain structure with a mean grain diameter of 26 μm (Fig. 1). In addition, the as-annealed material showed a sparse, random or non-uniform distribution of particles throughout the material identified by TEM analysis as HfO_2. Particles were between 0.2 and 0.4 μm in diameter with a monoclinic crystal structure. Twinning on the (100) was typically observed in the HfO_2 particles, as shown in Fig. 1(b).

While specific changes in the microstructure of the T-111 alloy occurred on aging the as-annealed material these further heat treatments did not produce any change to the measured mean grain diameter of the solid solution grains. In addition, the HfO_2 particles observed in the as-annealed material were retained in the samples following aging and showed no statistical increase in size or change in distribution of these retained particles. The small Zr concentration in the alloy was determined by EDS analysis to be segregated to the HfO_2 particles rather than remaining in the solid solution phase (Fig. 2). On the other hand, the concentration of W in the alloy was retained in the solid solution matrix and did not preferentially segregate to the HfO_2 particles. No particles were identified as either Zr- or W-base compounds in any of the conditions investigated.

SEM examination of the 1098 K aged material revealed only HfO_2 particles, remnants from the annealed condition (Fig. 3), and showed no evidence of grain boundary precipitation. TEM analysis (Fig. 4) of the 1098 K aged material confirmed that no precipitation along the grain boundaries had occurred. However, aging T-111 at 1098 K for 1100 h resulted in the development of rod-like structures, typically of 1 μm lengths and no more than 50 nm in thickness, distributed randomly throughout the solid solution matrix. These particles were observed as being both attached to the HfO_2

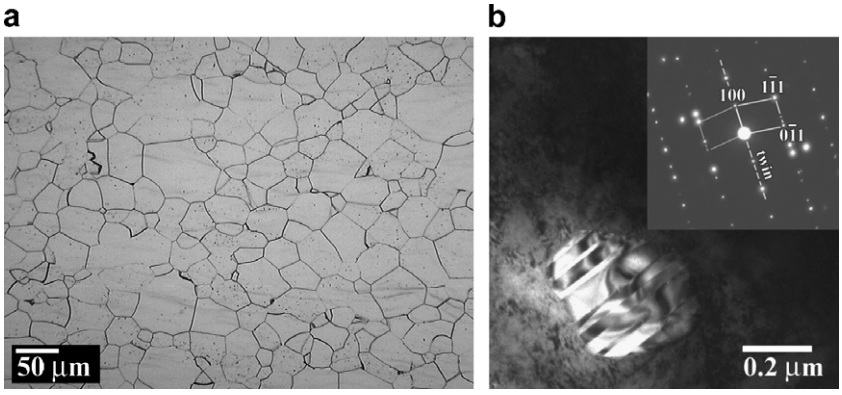

Fig. 1. (a) Optical micrograph of T-111 annealed 1 h at 1883 K, and (b) TEM image of HfO_2 particle with insert showing the (100) twin oriented [011] electron diffraction pattern taken from the particle.

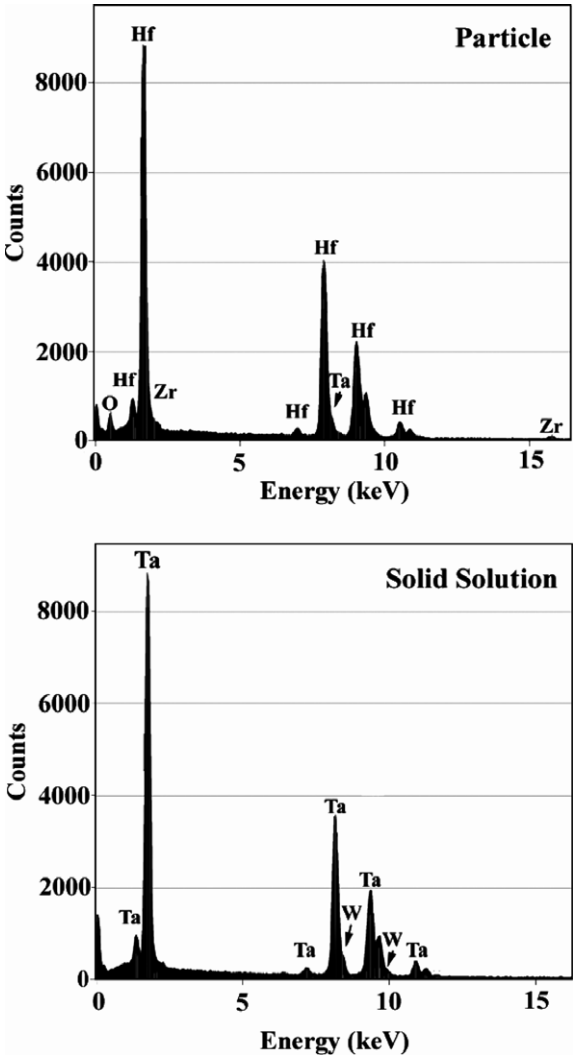

Fig. 2. Representative EDS spectra taken from an intergranular HfO_2 particle and the solid solution matrix, showing segregation of Zr and W to the particle and matrix respectively. The HfO_2 particle is a remnant of the as-annealed structure and is present in the same structure, size and distribution following all aging conditions.

particles as well as unattached (Fig. 4(a)). Closer examination of these features revealed an internal structure consisting of alternating twin planes (Fig. 5). Electron diffraction analysis (Fig. 6) indexed the rods as hexagonal in structure with lattice constants closely matching to the Ta_2N phase ($P6_3/mmc$, $a_o = 0.30445$ nm, $c_o = 0.49141$ nm). However, the Ta_2C phase shows a similar rhombohedral structure and lattice constants ($P\bar{3}m1$, $a_o = 0.31046$ nm, $c_o = 0.4944$ nm) that can be indexed using hexagonal convention. Efforts to determine the structure by the convergent beam electron diffraction technique were unsuccessful due to the small size of the individual twin variants contained within the rod. Twinning was observed on the $\{\bar{1}011\}$ planes with the rods aligned in the $\langle 1\,1\,0\rangle$ of the solid solution matrix. Analysis by EDS was also unsuccessful in determining the chemistry of the rods due to the small dimensional scale of the material and the background signal from the surrounding matrix. While a higher concentration of carbon over nitrogen was measured in the alloy through chemical analysis, the actual chemistry of the rods is uncertain.

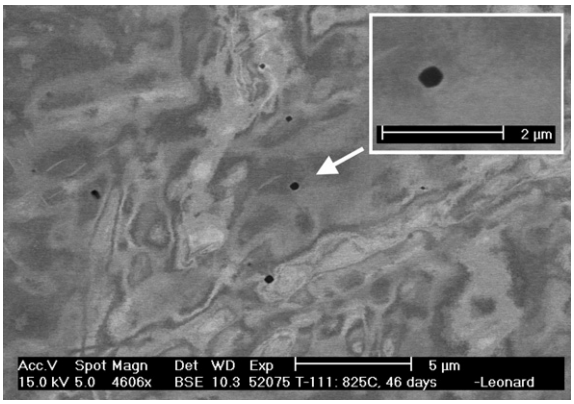

Fig. 3. Back-scatter SEM image of T-111 aged 1100 h at 1098 K. Faceted particles of HfO_2 are the remnants of the annealed structure.

Increasing the aging temperature resulted in precipitation along the grain boundaries in T-111. This was observed under back-scatter electron imaging in the SEM of the 1248 and 1398 K aged samples (Fig. 7). The amount of new precipitation in the material was restricted entirely to the grain boundaries with the size of the precipitates increasing with temperature. In addition, precipitate development at the grain boundaries in the 1398 K aged material resulted in the pinning of the migrating boundaries as is observed in the SEM image shown in Fig. 7(b). Though some boundary movement was observed in the sample, the mean grain size in the aged material showed no statistical change with respect to the as-annealed condition.

Precipitation at the grain boundaries of the 1248 K aged material was examined in more detail by TEM analysis (Fig. 8). The prepared TEM samples from the 1248 K aged material contained numerous grain boundaries and tri-junction locations for examination, from which it was evident that the precipitation on many of the boundaries was non-uniform in particle distribution, though

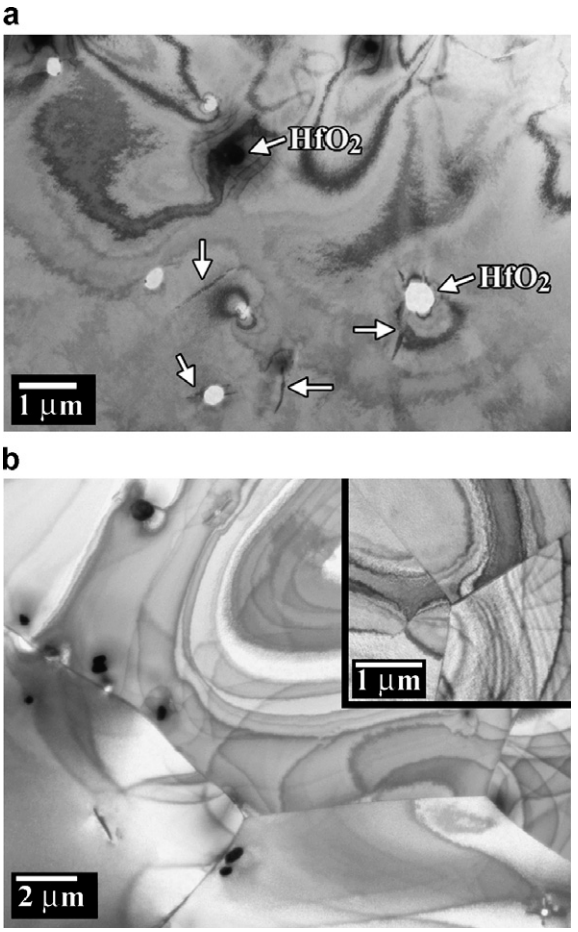

Fig. 4. TEM micrographs of T-111 aged 1100 h at 1098 K. (a) Image showing HfO_2 particles and unidentified rod-like particles (marked with arrows) in the solid solution. (b) Image showing grain boundary tri-junctions with insert showing a higher magnification image of another tri-junction location. Aging at 1098 K resulted in no observed precipitation along the grain boundaries with the exception of occasional HfO_2 particles from the annealing condition.

particle sizes were 50 nm or less. An example is shown in Fig. 8(a) where precipitation along the grain boundaries near a tri-junction varies from a dense distribution to a nearly precipitate free boundary extending away from the junction for at least 2.5 μm. However, typical precipitate development at the grain boundaries in the aged material was found to be similar to that shown in Fig. 8(b). The particles were determined by EDS to be Hf-rich, though the exact chemistry could not be determined. In addition, due to the small size of the particles, electron diffraction was unsuccessful in positively identifying the structure of the particles. Though intensities representing diffracted planes

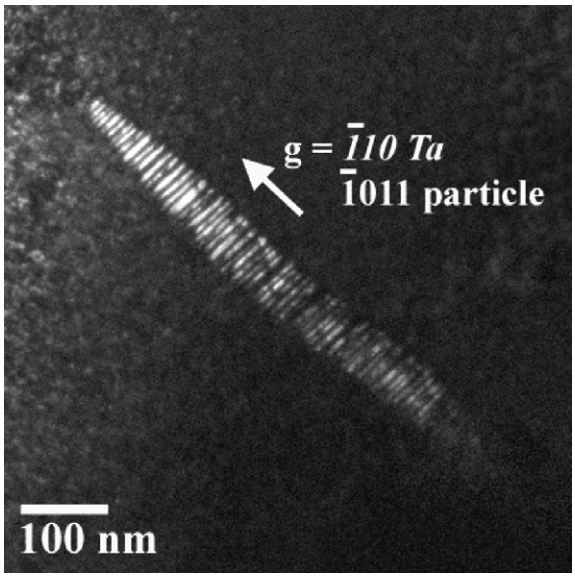

Fig. 5. Dark-field TEM image of a rod-like particle observed in material aged at 1098 K showing its twinned internal structure.

from the precipitate phase do appear within the diffraction patterns of the matrix grains, these intensities could be indexed to either the monoclinic, tetragonal or cubic variants of the HfO_2 phase. In addition to the grain boundary precipitate development, the 1248 K aged material also contained the same rod-like features as that of the 1098 K aged material (Fig. 8(c)). Again, these features showed an internal twinned structure. Electron diffraction analysis confirmed the structures to be hexagonal, with twinning occurring along the $\{1\bar{1}01\}$ planes (Fig. 8(d)). Interestingly, the $[11\bar{2}0]$ pattern shown in Fig. 8(d) was oriented with the Ta$[111]$ zone axis, which is different than that was observed in the 1098 K aged material. This difference was due to different growth directions of the rod-like particles along the $\langle 110\rangle$ variants in the Ta solid solution. In both aging conditions the particles showed twinning along the $\{1\bar{1}01\}$ planes which were aligned with the $\{110\}$ planes of the matrix.

TEM analysis of the 1398 K aged material is shown in Fig. 9. While the 1398 K aged material contained the remnant HfO_2 particles from the annealing condition, common to all conditions, the microstructure lacks the rod-like structures that were observed in the 1098 and 1248 K aged conditions. Extensive grain boundary precipitation occurred during aging at 1398 K. Unlike the 1248 K aged material, investigation of the grain boundaries in the 1398 K aged material revealed

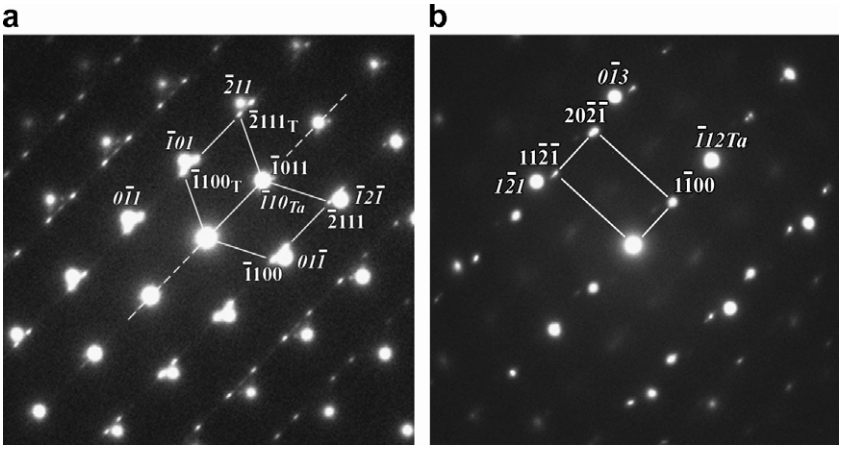

Fig. 6. SAD patterns from the rod-like features observed in material aged at 1098 K. Patterns were indexed to a hexagonal structured phase. (a) The Ta[1 1 1] rod[1 1 $\bar{2}$ 3] pattern showing twinning on $\{\bar{1}011\}$, and (b) the Ta[5 3 1] rod[1 1 $\bar{2}$ 6] pattern from one of the twinned variants in the particle. The indexed Ta solid solution planes are shown in italics, while that of a twin variant in the rod is marked with a 'T'.

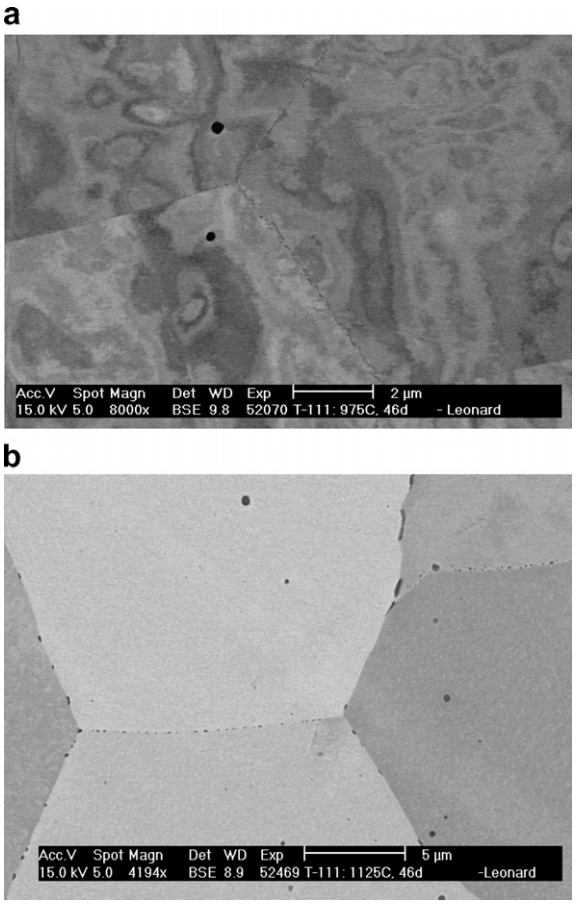

Fig. 7. Back-scatter electron images of T-111 aged 1100 h at (a) 1248 K and (b) 1398 K.

differences in the size and distributions of the precipitate particles on the boundaries. Particles ranged from large, widely separated precipitates of up to 0.6 μm in size (Fig. 9(a)), to smaller particles of 0.1 μm or less densely distributed along the grain boundaries (Fig. 9(c)). The larger particles were identified through EDS and their electron diffraction zone axis patterns as the monoclinic form of HfO_2 (Fig. 9(b)). Based on their size, the larger particles observed by TEM at the grain boundaries may have originated from the original annealing treatment. The angular appearance of these grain boundary precipitates, in contrast to the more rounded appearance of the intragranular HfO_2 particles in the sample and in the annealed material, suggests some further growth of the grain boundary precipitates during the aging. The lack of smaller particles near them may have been due to the depletion of Hf in the regions surrounding the grain boundary precipitates.

Convergent beam electron diffraction (CBED) was partially successful in determining the structure of the smaller precipitate particles in the 1398 K aged material. While EDS confirmed them to be Hf-rich, their chemistries were not clearly identifiable (i.e. oxide, carbide or nitride). Along one grain boundary, it was observed that the particles shared a common growth direction in one of the solid solution grains (Fig. 9(c)). The particles were determined to be cubic in structure with both the [1 0 0] and [1 1 0] zone axis identified, with the latter shown in Fig. 9(d). While the particles shared the same

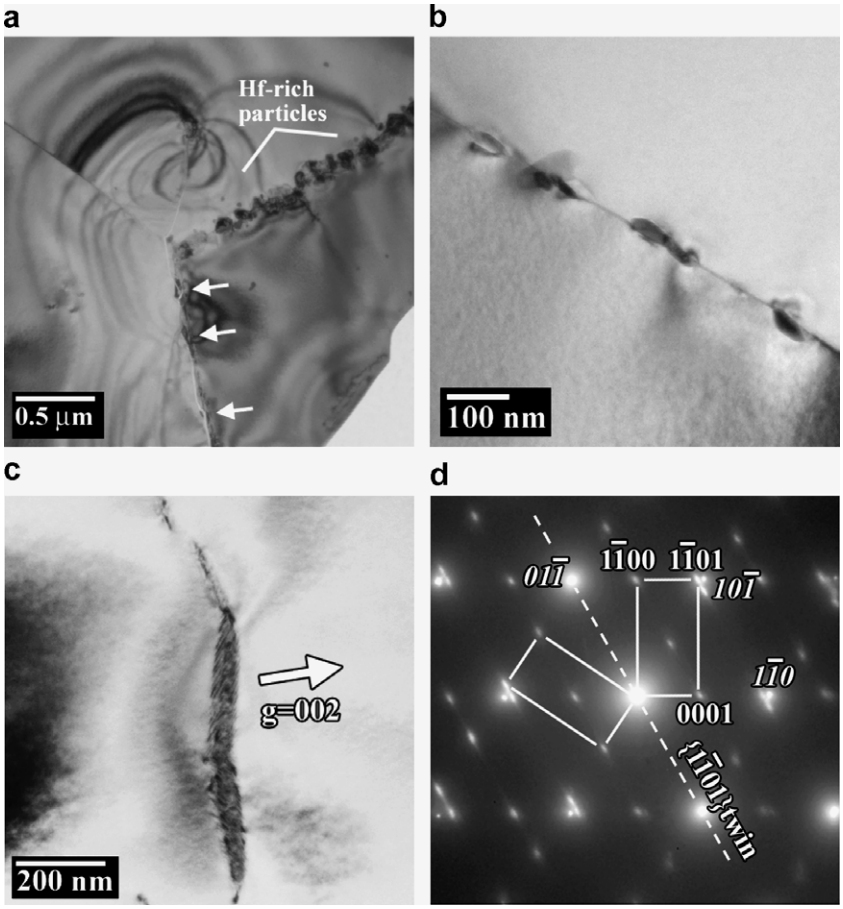

Fig. 8. TEM micrographs of 1248 K aged material. (a) Image showing the varied amount of precipitation of Hf-rich particles at a grain boundary tri-junction, with the micrograph in (b) showing more typical grain boundary precipitate formation. (c) Two-beam ($g = 002$) image showing rod-like features appearing in the solid solution matrix, and (d) the SAD pattern from the rod-like feature indexed to the hexagonal [$11\bar{2}0$] oriented to the Ta[111] zone (marked in italics) showing a {$1\bar{1}01$} twin oriented variant.

orientation, the ⟨200⟩ of the particles were slightly misaligned with respect to the ⟨110⟩ of the solid solution grain they grew into.

CBED analysis of the smaller precipitate particles located along different grain boundaries in the aged material indicated that variations in crystal structure occurred in the precipitates. An example of these particles is shown under dark-field imaging in Fig. 9(e), using several diffracting reflections from the precipitates to clearly view the degree of grain boundary decoration. In order to examine these differences further, a 200 μm diameter SAD aperture was used to provide diffraction information from the phases located in a 6.25 μm diameter area of the samples grain boundaries and tri-junction locations. This enabled the collection of diffracting planes from multiple particles along the boundaries in a pseudo ring-type pattern, an example of which is shown in Fig. 9(f). Reflections were indexed from the monoclinic and cubic forms of HfO_2 along with reflections from the solid solution grains forming the boundary.

While the monoclinic structure is stable below 1950 K in bulk material, the higher temperature tetragonal structure can be stabilized in submicron size particles [32], analogous to the more widely known tetragonal stabilization of ZrO_2 particles below 30 nm [33], due to a lower surface free energy than the monoclinic form. The cubic structure of HfO_2 is thermodynamically stable above 2473 K in bulk form and has not been reported previously in literature on nanoparticle or thin-film research. However, the cubic form of the oxide shares the same cubic $Fm\bar{3}m$ structure as HfN and HfC, as well as the reduced ZrO_{2-x} oxide and all have similar lattice constants. Therefore, it is possible that the cubic

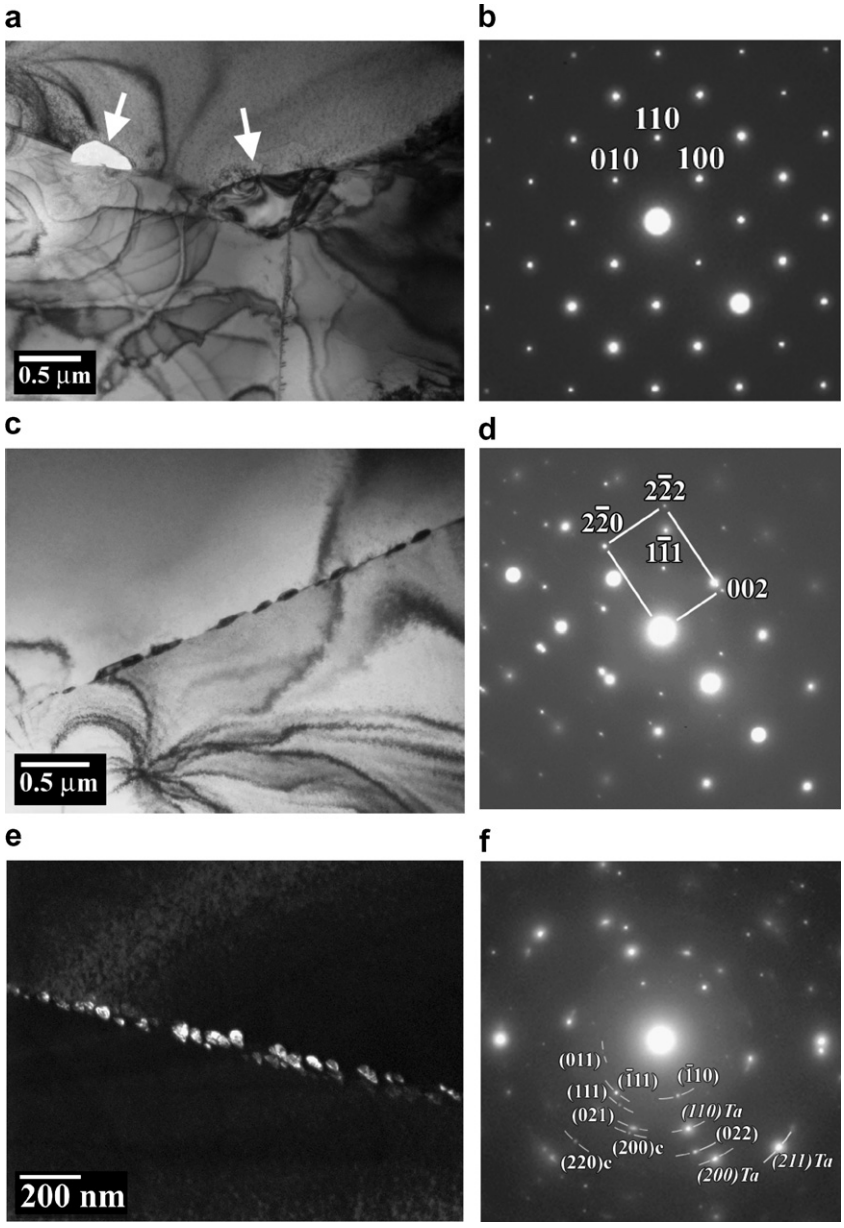

Fig. 9. TEM micrographs of T-111 aged 1100 h at 1398 K. (a) Large HfO_2 particles at a grain boundary tri-junction, marked by arrows, and (b) the SAD pattern of the monoclinic HfO_2 [0 0 1] zone axis of one of the particles shown in (a). (c) Bright-field image of precipitates along a grain boundary, with (d) the cubic [1 1 0] zone axis of a grain boundary precipitate nearly aligned to the [1 0 0] zone of the solid solution grain it is growing into. (e) Dark-field image grain boundary precipitates, with (f) a diffraction pattern from a large selected area of a typical grain boundary containing numerous particles with reflections corresponding to the monoclinic and cubic (marked with 'c') forms of HfO_2 with additional reflections from the Ta solid solution grains (marked with Ta in italics).

variants of the Hf-rich precipitates are mixed oxides containing carbon or nitrogen which has stabilized the crystal structure. The measured lattice constant of the cubic particles was 0.4596 ± 0.05 nm, which is between that of HfN and HfC (0.4525 and 0.4638 nm, respectively). Little and very mixed results are found in literature as to the preferential structure of HfO_2 nanoparticles, with indications that their structure may depend on the level and type of chemical impurities present in the material [32,34].

A general observation comparing the 1248 and 1398 K aged materials suggest that little difference

exists between the numbers of particles nucleated at the grain boundaries and that the higher temperature anneal resulted in an increase in particle size through coarsening. The development of grain boundary precipitation in T-111 on aging has a dramatic effect on the alloy's electrical and mechanical properties, as will be shown below.

3.2. Electrical resistivity

The room temperature electrical resistivity of the T-111 samples was measured in the as-received, annealed and aged conditions. The values of resistivity for each sample and the changes associated with aging of the samples at 1098, 1248 and 1398 K are listed in Table 2. No significant change in resistivity was measured between the as-received (cold worked) condition and that following annealing for 1 h at 1883 K. A change in resistivity is indicative of either a solute redistribution or a microstructural change occurring in the alloy, while changes in dislocations and grain size contribute little to the overall change in resistivity. While the as-annealed material did show a recrystallized structure of dislocation-free grains, the annealing temperature was not high enough to dissolve the HfO_2 particles, and may account for the lack of resistivity change between the annealed and cold-worked structures. The resistivity values of T-111 in this study following the various treatments are below the 217 nΩ m value reported in literature [9], but they are within ±5% of the average value.

A trend of decreasing resistivity is observed with increasing aging temperature, with averaged decreases of 3.7, 6.2 and 8.8 nΩ m measured between the annealed and 1098, 1248 and 1398 K aged samples, respectively. As earlier research on V–4Cr–4Ti alloys has demonstrated [35], resistivity changes of 10 nΩ m are as large as would be expected due to interstitial solute redistribution in the material without additional increases in impurity levels. Though an increase in nitrogen impurity was measured by chemical analysis following aging at 1398 K, an increase in electrical resistivity would have been expected if this increase was significant. The decreasing values of resistivity with increasing aging temperature correlate with the observed changes in microstructure. As more solute and interstitial are removed from solid solution into precipitates, the resistivity of bcc solid solution alloys decreases.

3.3. Hardness

The values of Vickers hardness following thermal treatment are presented in Table 3. A similar trend to electrical resistivity was observed, in that the hardness values decreased with increasing aging temperature. The decrease in hardness correlates with the precipitation of solute and interstitial elements along grain boundaries, resulting in a softening of the matrix. Despite the increased nitrogen content in the alloy following 1398 K aging, the average hardness is considerably less than that of the as-annealed material. The effect that interstitial impurity concentration has on the hardness of pure

Table 3
Averaged measured hardness of as-annealed and aged T-111 samples

Condition	Sample I.D.	Hardness (kg/mm^2)
Annealed 1 h at 1883 K	T120	253 ± 3
Annealed + Aged 1100 h at 1098 K	T134	241 ± 4
Annealed + Aged 1100 h at 1248 K	T135	236 ± 3
Annealed + Aged 1100 h at 1398 K	T139	235 ± 1

Table 2
Room temperature electrical resistivity (nΩ m) of T-111 in the as-received, annealed and aged conditions

Sample I.D.	As-received resistivity	As-annealed resistivity	Resistivity after 1100 h aging at:			Difference (Aged − Annealed)
			1098 K	1248 K	1398 K	
T132	200.9	201.7	197.7			−4.0
T133	203.6	204.0	201.5			−2.5
T134	202.6	203.8	199.2			−4.6
T135	202.2	203.3		196.9		−6.4
T136	201.5	202.2		196.1		−6.1
T137	202.3	203.0		196.9		−6.1
T138	201.0	201.2			192.3	−8.9
T139	202.3	202.7			195.8	−6.9
T140	203.4	203.6			193.0	−10.6

Ta has been investigated, with data compiled and presented in Refs. [1,36]. These data showed that a linear increase in hardness occurs with the addition of oxygen or nitrogen until saturation at levels of 3600 and 6600 wppm respectively. From these data, a net increase of 85 wppm nitrogen occurring in the 1398 K aged material should produce an insignificant increase in hardness. The similar hardness values between the 1248 and 1398 K aged samples may reflect the coarsening of the precipitates on the grain boundaries between these two temperatures more than an increase in the nucleation of new particles. Taken together, the microstructure, resistivity and hardness data suggest that aging for 1100 h causes progressively enhanced precipitation of Hf-rich precipitates (assumed to be mixed oxide, carbide, nitride composition), with preferential nucleation along grain boundaries. The formation of the grain boundary precipitates reduces the matrix interstitial solute content and thereby causes overall softening of the matrix.

3.4. Tensile properties

Tensile properties for the annealed and aged material are presented in Table 4. The increasing precipitate development along the grain boundaries with increasing aging temperature led to a reduction in the tensile strength of the aged material, compared to the as-annealed condition, and to pronounced tensile embrittlement in the 1398 K aged material as monitored by uniform and total elongation and reduction in area.

The tensile properties of the as-annealed material showed good ductility at all temperatures with values of total elongation remaining above 20%. Only a small decrease in yield strength (YS) was measured between the elevated temperature tests of the as-annealed material. The tensile properties of T-111 have been collected by Zinkle [37] from open literature [1,8,9], and correlations were developed by him as a function of temperature for the YS and ultimate tensile strength (UTS). The correlations are shown in Fig. 10 for both UTS and YS, along with the data of this study. The UTS of the annealed T-111 specimens of this study consistently lie above the correlation at all temperatures while that for the aged specimens at 1073 and 1223 K are quite close to the correlation curve. The UTS for the samples aged at 1398 K is below the correlation, but that is expected as this condition was highly embrittled. The YS measured for the annealed and aged samples are close to the correlation at all temperatures. The large difference between the YS and UTS of the samples indicate a high level of work-hardening (which is also apparent in the stress–strain curves) and is consistent with the data from open literature. Sheffler et al. [2] studied the strain aging behavior of T-111 and reported that the high strength (relative to pure Ta) may be caused by a complex atmosphere–dislocation interaction rather than by simple interstitial dislocation pinning. During aging, as the interstitial elements are redistributed and precipitated, the complex atmosphere–dislocation interactions weaken and the UTS drops. As the rate of diffusion increases with increasing temperature, a reduction in work hardening is expected, as was observed in the results of this study.

The stress–strain curves for the 1098 K aged and annealed samples tested at 1073 K are shown in

Table 4
Tensile properties of annealed and 1100 h aged T-111

Test temperature (K)	Condition	Sample I.D.	YS (MPa)	UTS (MPa)	Uniform elongation (%)	Total elongation (%)	Reduction in area (%)
RT	Annealed	T104	699	787	15.4	29.2	–
1073	Annealed	T112	277	580	12.9	21.2	65.1
	Aged 1098 K	T132	247	465	15.3	24.5	49.4
	Aged 1098 K	T133	250	460	13.2	21.2	–
1223	Annealed	T131	269	523	15.2	26.4	71.1
	Aged 1248 K	T135	240	447	12.9	24.1	49.2
	Aged 1248 K	T136	223	470	9.4	16.9	53.6
1373	Annealed	T128	246	492	14.1	23.1	49.9
	Aged 1398 K	T138	220	338	1.0	7.2	13.5
	Aged 1398 K	T139	240	311	0.8	6.6	10.4
	Aged 1398 K	T140	235	281	1.5	5.9	2.2[a]

[a] Sample failed in shoulder, with reduction in area calculated based on original gage cross-section.

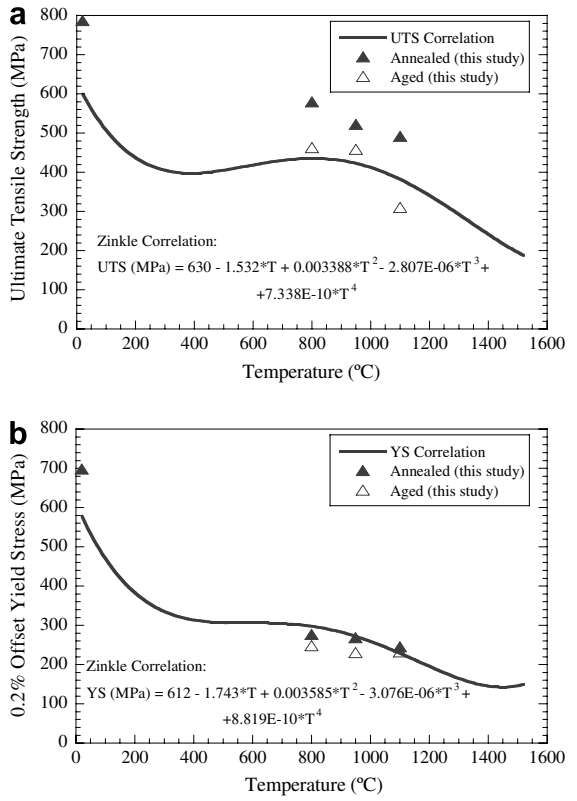

Fig. 10. Comparison of the (a) ultimate tensile strength and (b) yield stress correlations developed by Zinkle for T-111 [37] and the tensile data from this study.

Fig. 11(a). Both 1098 K aged samples showed a significant reduction in tensile strengths compared to the as-annealed condition, with a measured reduction of over 100 MPa in UTS. The observed softening during aging correlates with the reduction in both electrical resistivity and hardness. Dynamic strain aging (DSA) was exhibited in both the aged and annealed conditions, although the nature of the DSA was very different for the two conditions. In the annealed material, serrations do not appear until after the maximum load has been reached (>15% elongation) and the specimen has started to neck. The onset of dynamic strain aging was marked by a drop in stress, as shown in the more detailed stress–strain curve in Fig. 11(b). The 1098 K aged specimen exhibited DSA for elongations greater than 7–8%. The serrations in the aged sample are primarily load drops, indicating a Type A dynamic strain aging [38,39], similar to that occurring in the annealed specimen following the initial drop in stress.

The difference in DSA behavior and reduction in strength of the aged specimens from the as-annealed are indicative of microstructural difference between the two conditions relating to the distribution of impurities in the material, as overall impurity levels between the two conditions are similar (Table 1). While resistivity, hardness and tensile strength suggest reduced interstitial solute in the matrix of the aged samples compared to the as-annealed, the early onset of DSA in the aged sample suggests the opposite. In terms of microstructure, both the as-annealed and 1098 K samples showed HfO_2 particles distributed inhomogeneously throughout the microstructure, with the only difference observed between the samples being the presence of the rod-like features distributed throughout the solid solution grains in the aged material. Though relatively low in distribution density (1.6×10^{18} particles/m^3), the precipitation of these features may have an influence on mechanical properties as well as on electrical resistivity. Furthermore, the stability of these rod-like features with temperature is not known. Though appearing in both the 1098 and 1248 K samples, they may have formed during cooling and therefore release their solute contents at the tensile test temperatures. Whereas, aging at 1398 K may have been high enough to reduce the solute and interstitial content of the solid solution matrix, that no rod-like features were observed during post-aging examination. The delay of DSA in the annealed material until reaching the UTS could be attributed to the binding of carbon and oxygen in the solid solution, whereas oxygen in the aged material is tied up in precipitates allowing for the carbon in the aged material to interact more freely with the dislocations. A higher level of interstitial concentration in the solid solution which is not tied to precipitates has been shown to produce strain aging effects in steels with similar overall levels of impurity concentrations [40].

Fractography of the 1098 K aged and annealed specimens tested at 1073 K are compared in Fig. 12(a). Both samples exhibit ductile–dimple failure. Although the aged specimen has a lower reduction of area than the annealed specimen, both samples have sufficiently high values.

The stress–strain curves for the 1248 K aged and annealed T-111 specimens tested at 1223 K are shown in Fig. 11(c). Similar to the samples tested at 1073 K, the results for both aged specimens indicate a lower YS and UTS than the annealed specimens. In addition to a drop in strength, there is also a slight drop in uniform elongation from the values for the annealed condition. However, the

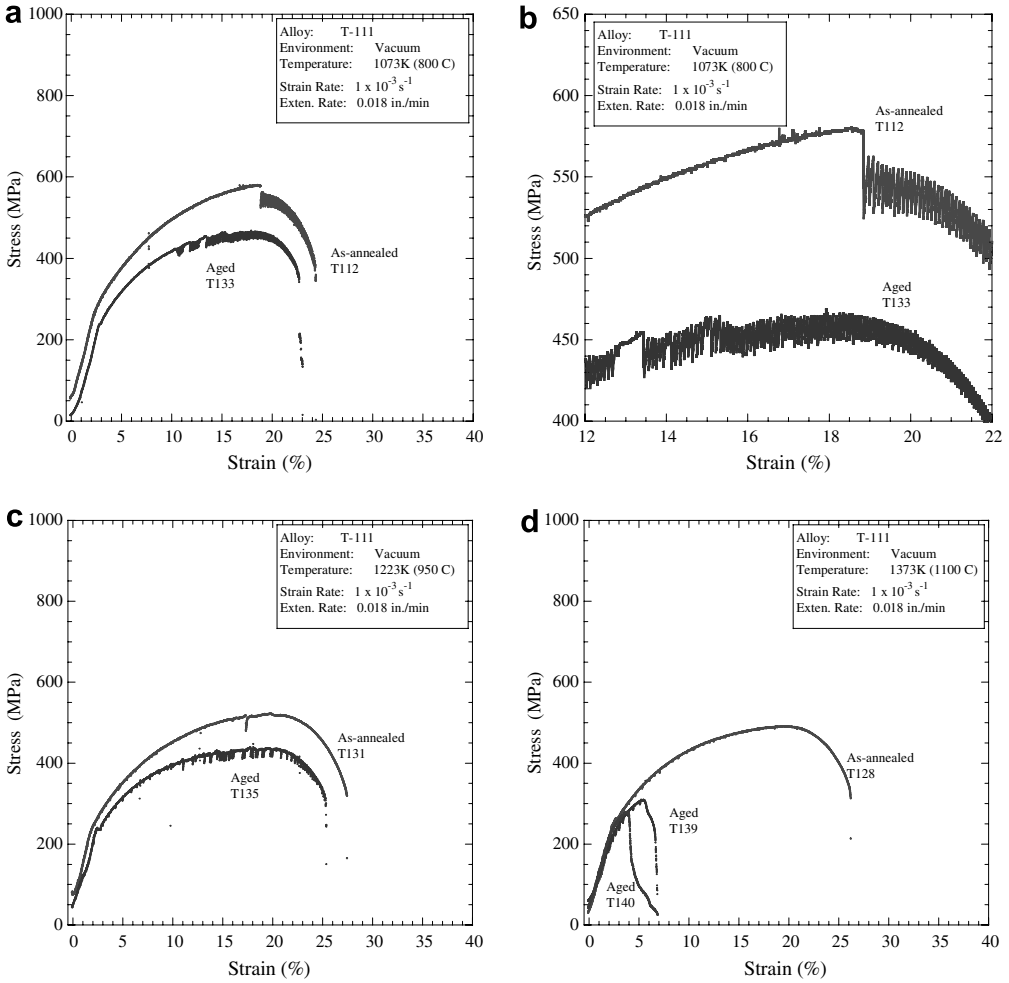

Fig. 11. Comparison of the stress–strain curves for 1100 h aged and annealed T-111 samples. (a) 1098 K aged and as-annealed samples tested at 1073 K with (b) detail of dynamic strain aging occurring in those samples. (c) 1248 K aged and as-annealed samples tested at 1223 K, and (d) 1398 K aged and as-annealed samples tested at 1373 K.

values of uniform and total elongation as well as the reduction in area are acceptably high and indicative of ductile, structural materials. Though DSA is present in both the 1248 K aged and annealed samples tested at 1223 K, it is much less pronounced in the annealed specimen. In addition, the serrations which are also Type A are considerably less frequent than in the 1098 K aged specimens, but are occurring shortly after yielding.

Fractography of the 1248 K aged and annealed specimens tested at 1223 K are compared in Fig. 12(b). The annealed specimen failed in a ductile mode with over 71% reduction in area. However, the aged specimens exhibited a mixed failure mode with regions of intergranular (IG), transgranular (TG) and ductile failure. Overall, the fracture surface for aged samples was 52% IG/TG for sample T135 (not shown) and 83% IG/TG for sample T136.

The stress–strain curves for the 1398 K aged and annealed T-111 specimens tested at 1373 K are shown in Fig. 11(d). All three aged samples failed prematurely with uniform elongations of less than 1.5%. The aged specimens exhibited a UTS 150 to 200 MPa lower than for the annealed specimens due to their low uniform elongation. However, the measured yield stresses varied only slightly between the annealed and 1098 K aged material tested at 1373 K. Fractography of the 1398 K aged and annealed specimens tested at 1373 K are compared in Fig. 12(c). All three aged specimens exhibited both IG and ductile features although the samples were predominantly (75–88%) IG. The increased

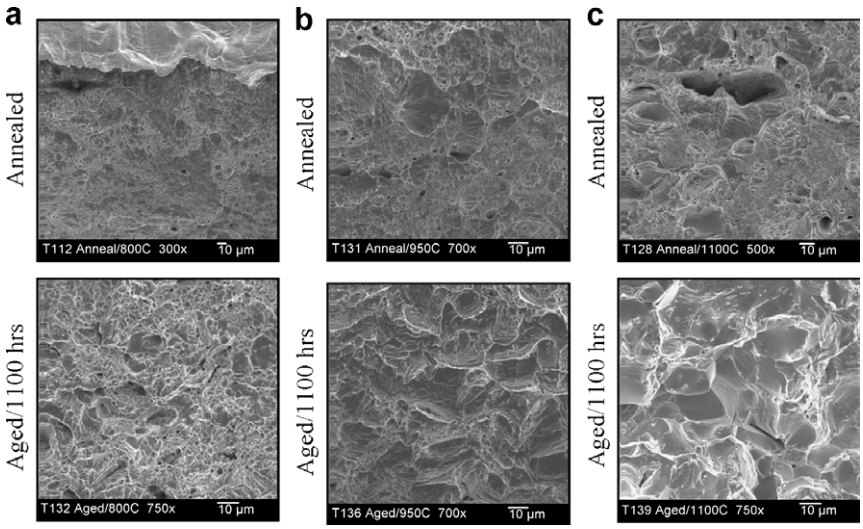

Fig. 12. Comparison of fracture surfaces of annealed and aged T-111 samples tested at (a) 1073 K, (b) 1223 K and (c) 1373 K.

N content in the samples following aging at 1398 K may have some influence on the mechanical behavior of the specimens. However, it does not fully explain the extent of degradation of T-111 after aging. Indeed, all the aged specimens showed signs of softening or loss of tensile strength after aging, with the degree of degradation increasing with increasing aging temperature. However, there was no measurable impurity pickup following aging at 1098 or 1248 K. The possibility also remains that the single value showing high N may be an anomaly or an artifact of material sampling for chemical analysis. Clear indications of solute segregation to the grain boundaries as a result of thermally-driven processes leading to the increased development of precipitates with increasing aging temperatures are apparent and have a detrimental affect on mechanical properties of the alloy.

A review of literature shows some differing results in terms of embrittlement appearing in aged T-111. In work by Lessmann and Gold [24,41], aging at 1255, 1422 and 1588 K for times up to 10 000 h did not produce any change in the bend test DBTT. Tensile data [41] of aged sheet material taken at these temperatures under similar test conditions as the data presented in this article, showed ductility greater than 20% total elongation, except at 1255 K which showed values exceeding 10%. No indications of embrittlement with aging were reported. Conversely, a decrease in bend test ductility was reported by Stephens [22,23] for T-111 tube annealed at 1925 K and aged at 1315 K for 1000 h in vacuum and lithium environments. This embrittlement was only found to occur over a narrow temperature range for T-111, with no embrittlement observed in materials aged at 1200 and 1425 K. Tensile tests by Stephens on 1313 K aged material tested at temperature did show a decrease in UTS compared to the annealed condition and similar values of yield strength between the two conditions, though embrittlement was not reported to have occurred in the tested material. However, values for tensile ductility were not reported. The source of embrittlement in bend test data by Stephens, was suggested to be the result of HfO_2 particle development at the grain boundaries. Further work by Stephens showed that the mechanical properties and response to aging was an effect of Hf and W concentrations in the alloy, in that embrittlement was not observed when the level of Hf was reduced to 0.5–1.0% or the amount of W reduced to 4%. It was proposed by Stephens that Hf segregation to the grain boundaries is enhanced by W additions to the alloy through a lattice contraction that occurs when W is added to Ta, leading to greater misfit strains around the Hf atoms in the solid solution. The embrittlement reported by Stephens as occurring in T-111 at 1315 K, did not appear in similarly aged and tested Ta–10 W or Ta–2Hf.

4. Conclusions

The microstructural changes and their effect on the electrical and mechanical properties of T-111 following 1100 h aging at 1098, 1248 and 1398 K

have been investigated. Increasing aging temperatures caused a measurable decrease in electrical resistance and sample hardness due to the precipitation of Hf-rich compounds at the grain boundaries. The increased amount of precipitate development at the grain boundaries with increasing temperature appears to be responsible for the reduction in material strength by reducing the interstitial solute concentration on the matrix. In addition, the grain boundary precipitates appear to be responsible for tensile embrittlement of the alloy following aging at 1398 K. Precipitation at the grain boundaries was found to be a mixture of monoclinic and cubic structures, suggesting the development of mixed Hf oxides, carbides and nitrides. It is not known whether variations in the annealing temperature or pre-aging treatments can influence or lessen the amount of solute segregation to the grain boundaries. While the mechanical properties following aging at 1398 K may have been influenced by the 90 wppm increase in nitrogen due to a pinhole leak in the container during aging, general trends indicating microstructural instability are observed with increasing aging temperature. Further work is necessary to evaluate the microstructural stability of the material over longer times, to examine the amount of precipitate coarsening at the grain boundaries and its influence on mechanical properties.

Acknowledgements

The authors thank J. Hack, R. Baranwal, T.M. Angeliu and Y. Ballout of the Naval Reactors Prime Contractor Team for many helpful technical discussions and guidance. The authors thank Marie Williams, Mike Pershing and Cliff Davison for help in acid cleaning and annealing of the specimens prior to thermal aging; Jeffrey McNabb and Bob Sitterson for welding and leak testing the Alloy 600 aging cans; Brian Sparks and David Harper for thermal aging the encapsulated materials; Kathy Thomas and Jackie Mayotte for their help in preparing samples for microscopy. The authors thank Chad Duty and Bill Wiffen for their helpful discussions. This work was performed under the sponsorship of NASA's Project Prometheus and directed by DOE/NNSA Naval Reactors. Opinions and conclusions drawn by the authors are not endorsed by DOE/NNSA Naval Reactors. Research at the Oak Ridge National Laboratory SHaRE User Center was sponsored by the Division of Materials Sciences and Engineering, US Department of Energy. ORNL is managed for DOE by UT-Battelle, LLC, under contract DE-AC-05-00OR22725.

References

[1] T.E. Tietz, J.W. Wilson, Behavior and Properties of Refractory Metals, Stanford University, Stanford, CA, 1965.
[2] K.D. Sheffler, J.C. Sawyer, E.A. Steigerwald, Trans. Am. Soc. Met. 62 (1969) 749.
[3] K.D. Sheffler, J. Vac. Sci. Technol. 8 (6) (1971) 58.
[4] G.T. Gray III, A.D. Rollett, The High-Strain Rate and Spallation Response of Tantalum, Ta–10W and T-111, LA-UR-91-3160, 1991.
[5] R.W. Buckman Jr., in: C.L. Briant et al. (Eds.), MRS Symposium Proceedings, Materials Research Society, vol. 322, 1994, p. 329.
[6] S.R. Chen, G.T. Gray III, Metall. Mater. Trans. A 27A (1996) 2994.
[7] J.R. DiStefano, H.E. McCoy, Int. J. Refract. Met. Hard Mater. 20 (2002) 381.
[8] F.W. Wiffen, in: R.J. Arsenault (Ed.), Proceedings of International Conference on Defects and Defect Clusters in BCC Metals and Their Alloys, Nuclear Metallurgy, vol. 18, National Bureau of Standards, 1973, p. 176.
[9] D.C. Goldberg, in: W.F. Brown Jr. (Ed.), Aerospace Structural Metals Handbook, AFML-TR 68-115, 9, Metals and Ceramics Information Center, Battelle Columbus Laboratories, 1969.
[10] R.W. Buckman, JOM 52 (3) (2000) 40.
[11] R.W. Buckman Jr., R.C. Goodspeed, in: I. Machlin, R.T. Begley, E.D. Weisert (Eds.), Refractory Metal Alloys Metallurgy and Technology, Plenum, New York, NY, 1968, p. 373.
[12] R.W. Buckman Jr., Am. Vac. Soc. (1996) 25.
[13] K.D. Sheffler, J. Vac. Sci. Technol. 8 (6) (1971) 58.
[14] R.W. Buckman Jr., Int. J. Refract. Met. Hard Mater. 18 (2000) 253.
[15] E.E. Hoffman, in: M.S. El-Genk, M.D. Hoover (Eds.), Space Nuclear Power Systems 1984, 1985, p. 349.
[16] R.E. Cleary, Corrosion Studies of Refractory Metals in Lithium, AEC-NASA Liquid Metals Information Meeting, USAEC Report CONF-650411, US Atomic Energy Commission, 1965.
[17] J.H. DeVan, J.R. DiStefano, E.E. Hoffman, in: R.H. Cooper Jr., E.E. Hoffman (Eds.), Proceedings of Symposium on Refractory Alloy Technology for Space Nuclear Power Applications, CONF-8308130, Oak Ridge National Lab, Oak Ridge, TN, 1984, p. 34.
[18] R.G. Donnelly, Welding of Refractory Alloys, High-Temperature Materials Program Progress Report for Period Ending July 31, 1965, ORNL-TM-1200, p. 7, and ORNL-TM-1140, 1965, p. 10.
[19] G.G. Lessmann, D.R. Stoner, in: 9th National SAMPLE Symposium on Joining of Materials for Aerospace Systems, Dayton, Ohio, November 1965.
[20] G.G. Lessmann, in: R.H. Cooper Jr., E.E. Hoffman (Eds.), Proceedings of Symposium on Refractory Alloy Technology for Space Nuclear Power Applications, CONF-8308130, Oak Ridge National Lab, Oak Ridge, TN, 1984, p. 146.
[21] G.K. Watson, J.R. Stephens, Effects of Aging at 1040 °C (1900 °F) on the Ductility and Structure of a Tantalum

Alloy, T-111, NASA TN D-6988, NASA Lewis Research Center, Cleveland, OH, 1972.
[22] J.R. Stephens, J. Less Common Met. 51 (1977) 93.
[23] J.R. Stephens, in: M.S. El-Genk, M.D. Hoover (Eds.), Space Nuclear Power Systems 1986, 1986, p. 291.
[24] G.G. Lessmann, R.E. Gold. Thermal Stability of Refractory Metal Alloys, NASA-SP-245, Westinghouse Astronuclear Laboratory, Pittsburgh, PA, 1970.
[25] R.W. Buckman, in: R.H. Cooper Jr., E.E. Hoffman (Eds.), Proceedings of Symposium on Refractory Alloy Technology for Space Nuclear Power Applications, CONF-8308130, Oak Ridge National Lab, Oak Ridge, TN, 1984, p. 86.
[26] T.G. Nieh, J. Wadsworth, in: C.L. Briant et al. (Ed.), High Temperature Silicides and Refractory Alloys, MRS Symposium Proceedings, Materials Research Society, vol. 322, 1984, p. 315.
[27] ORNL Standard Operating Procedure, MET-IHS-SOP-O1, Ta-10W Degreasing and Acid Cleaning, 2004.
[28] J.T. Busby, K.J. Leonard, L.L. Snead, F.W. Wiffen, S.J. Zinkle, J. Nucl. Mater., these Proceedings, doi:10.1016/j.jnucmat.2007.03.028.
[29] Standard Test Method for Resistivity of Electrical Conductor Materials, ASTM Designation B 193-87, ASTM Standards Online, American Society for Testing and Materials, Philadelphia, PA, 1992.
[30] A. Buch, Pure Metal Properties: A Scientific Technical Handbook, ASM International and Freund Publishing House Ltd., Materials Park, OH, 1999.
[31] Standard Test Method for Tension Testing of Metallic Materials, ASTM standard E8-04, ASTM Standards Online, American Society for Testing and Materials, Philadelphia, PA, 2001.
[32] J. Tang, J. Fabbri, R.D. Robinson, Y. Zhu, I.P. Herman, M.L. Steigerwald, L.E. Brus, Chem. Mater. 16 (2004) 1336.
[33] (a) R.C. Garvie, J. Phys. Chem. 69 (1965) 1238;
(b) R.C. Garvie, J. Phys. Chem. 82 (1978) 218.
[34] S.J.L. Ribeiro, Y. Messaddeq, R.P. Gonçalves, M. Ferrari, M.A. Aegerter, Appl. Phys. Lett. 77 (22) (2000) 3502.
[35] (a) M. Li, D.T. Hoelzer, S.J. Zinkle, Electrical Resistivity Data of Vanadium Alloys in the RB-17J Experiment, Fusion Materials Semi-Annual Report, DOE/ER-0313/34, June 2003, p. 2;
(b) S.J. Zinkle, A.N. Gubbi, W.S. Eatherly, Electrical Resistivity of V–Cr–Ti Alloys, Fusion Materials Semi-Annual Report, DOE/ER-0313/21, December 1996, p. 15.
[36] W.D. Wilkinson, Properties of Refractory Metals, Gordon and Breach Science Publishers Inc., New York, NY, 1969.
[37] S.J. Zinkle, Thermophysical and Mechanical Properties for Ta–8%W–2%Hf, Fusion Materials Semi-Annual Report, December 1999, DOE/ER-0313/27, p. 175.
[38] R. Abbaschian, in: Physical Metallurgy Principles, 2nd Ed., PWS Publishing Company, Boston, MA, 1994, p. 296.
[39] R.B. Schwarz, L.L. Funk, Acta Metall. 33 (1985) 295.
[40] Y. Tomota, P. Lukas, S. Harjo, J-H. Park, N. Tsuchida, D. Neov, Acta Mater. 51 (2003) 819.
[41] G.G. Lessmann, R.E. Gold. Long-Time elevated Temperature Stability of Refractory Metal Alloys, WANL-PR-(P)-014, Westinghouse Astronuclear Laboratory, Pittsburgh, PA, 1969.